www.afm-journal.de

ADVANCED FUNCTIONAL MATERIALS

RESEARCH ARTICLE

Turning Normal to Abnormal: Reversing CO_2/C2-Hydrocarbon Selectivity in HKUST-1

Mona H. Mohamed, Islam Elzeny, Joshua Samuel, Wenqian Xu, Christos D Malliakas, Yoosuf N. Picard, Tony Pham, Lenore Miller, Adam Hogan, Brian Space, David Hopkinson, and Sameh K. Elsaidi**

Metal–organic frameworks (MOFs) can efficiently purify hydrocarbons from CO_2, but their rapid saturation, driven by preferential hydrocarbon adsorption, requires energy-intensive adsorption–desorption processes. To address these challenges, an innovative approach is developed, enabling control over MOF flexibility through densification and defect engineering, resulting in an intriguing inverse CO_2/C2 hydrocarbon selectivity. In this study, the densification process induces the shearing of the crystal lattice and contraction of pores in a defective CuBTC MOF. These changes have led to a remarkable transformation in selectivity, where the originally hydrocarbon-selective CuBTC MOF becomes CO_2-selective. The selectivity values for densified CuBTC are significantly reversed when compared to its powder form, with notable improvements observed in CO_2/C_2H_6 (4416 vs 0.61), CO_2/C_2H_4 (15 vs 0.28), and CO_2/C_2H_2 (4 vs 0.2). The densified material shows impressive separation, regeneration, and recyclability during dynamic breakthrough experiments with complex quinary gas mixtures. Simulation studies indicate faster CO_2 passage through the tetragonal structure of densified CuBTC compared to C_2H_2. Experimental kinetic diffusion studies confirm accelerated CO_2 diffusion over hydrocarbons in the densified MOF, attributed to its small pore window and minimal interparticle voids. This research introduces a promising strategy for refining existing and future MOF materials, enhancing their separation performance.

M. H. Mohamed, I. Elzeny, J. Samuel, S. K. Elsaidi
Department of Chemistry
Illinois Institute of Technology
Chicago, IL 60616, USA
E-mail: mmohamed3@iit.edu;selsaidi@iit.edu
M.H.Mohamed,S.K.Elsaidi

SE-MATSmartlyEngineeredMaterialsLLC
Pittsburgh,PA15238,USA
M.H.Mohamed
DepartmentofChemistry,FacultyofScience
AlexandriaUniversity
AlexandriaEgypt
W.Xu
X-rayScienceDivision,AdvancedPhotonSource
ArgonneNationalLaboratory
Lemont,IL60439,USA

C. D Malliakas
Department of Chemistry
Northwestern University
Evanston, IL 60208, USA
Y. N. Picard, D. Hopkinson
DOE National Energy Technology Laboratory (NETL)
Pittsburgh, PA 15236, USA
Y. N. Picard
Oak Ridge Institute for Science and Education
Pittsburgh, PA 15236, USA
T. Pham

The ORCID identification number(s) for the author(s) of this article can be found under https://doi.org/10.1002/adfm.202312280

DOI: 10.1002/adfm.202312280

1. Introduction

The removal of carbon dioxide (CO_2) impurities from hydrocarbons is a crucial step in industrial processes, enhancing the quality and purity of the hydrocarbon feedstock for diverse applications like chemicals, fuels, and plastics.[1] This contributes to reducing the overall carbon footprint and promotes sustainability in the industry.[2] Physical adsorption has been identified as a more energy-efficient approach for gas separation compared to traditional cryogenic distillation or liquid extraction methods.[3] Nonetheless, developing CO_2-selective adsorbents is challenging due to the similarities in molecular dimensions and physical properties between C2-hydrocarbons and CO_2.

Metal–organic frameworks (MOFs) have been extensively studied in this regard, demonstrating selective adsorption of hydrocarbons over CO_2 "normal selectivity" using mechanisms like acid–base interactions, hydrogen bonds, functional groups, and open metal sites.[4] However, the rapid filling of the material by the dominant

Department of Chemistry
University of South Florida Tampa,
FL 33620, USA
L. Miller, A. Hogan, B. Space Department of Chemistry
North Carolina State University Raleigh,
NC 27607, USA

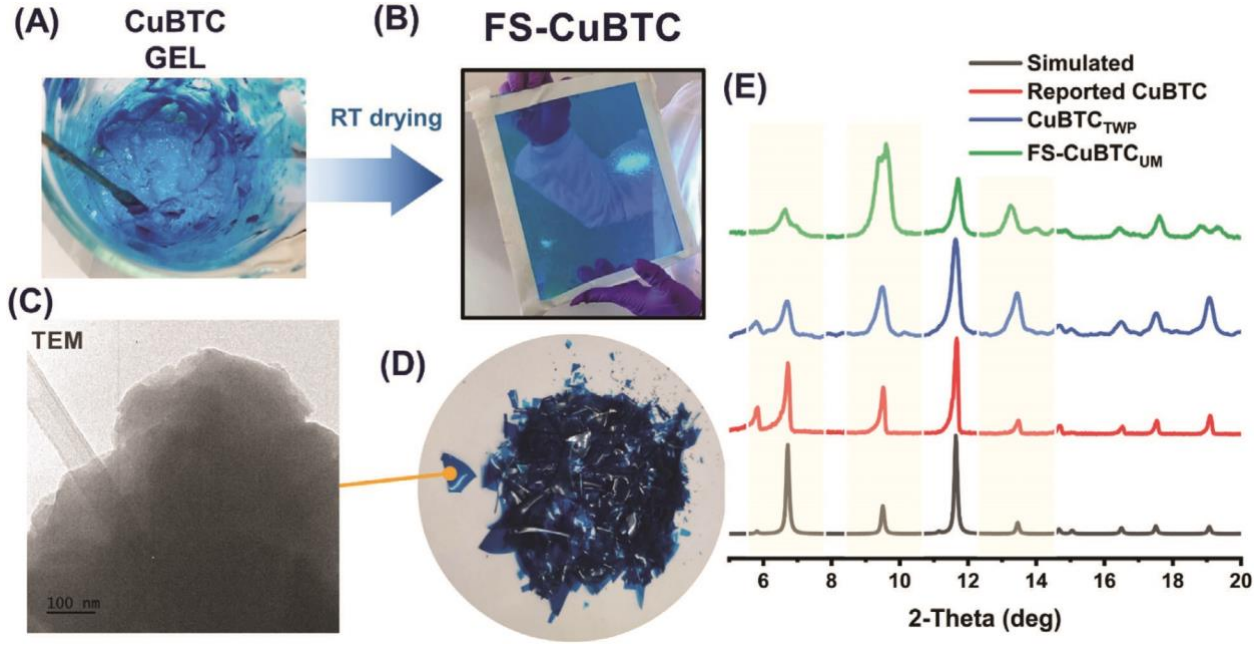

Figure 1. A) the CuBTC gel material, B) the FS-CuBTC on a glass sheet, C) the TEM image of the FS-CuBTC, D) the kilogram-scale of the FS-CuBTC, and E) PXRD patterns of the CuBTC$_{TWP}$ and FS-CuBTC$_{UM}$ compared with the simulated and reported CuBTC.

hydrocarbon component leads to time lags and necessitates two energy-intensive steps: adsorption followed by desorption.

An energy-efficient alternative is to achieve pure hydrocarbon separation in a single step using an adsorbent with "inverse selectivity," preferentially adsorbing CO_2 over hydrocarbons. This inverse selectivity has been observed in some reported MOFs. In the literature, it has been observed that the manipulation of MOF structural flexibility is a common reason behind the observed inverse selectivity, which enables the preferential adsorption of certain guest molecules based on pore size and geometry. For instance, Kitagawa and coworkers[5] demonstrated that [Mn(bdc)(dpe)], a flexible MOF material, selectively captured CO_2 from a mixture of CO_2 and C_2H_2, with a selectivity of 8.8 at 273 K and 1.0 bar. The flexible $[Zn(odip)_{0.5}(bpe)_{0.5}(CH_3OH)]\cdot 0.5NMF\cdot H_2O$ MOF has also shown an inverse selectivity of CO_2/C_2H_2 of 13.2.[6] Similarly, a family of lanthanide frameworks assembled with flexible acylamide ligands exhibited highly selective CO_2 capture compared to C_2H_6 or C_2H_4 at 273 K and ambient pressure.[7] This selectivity resulted from the interaction of CO_2 with the framework and the structural flexibility, allowing exclusive recognition of CO_2 without the co-adsorption of other gases.

Here, we present a new strategy to control the flexibility of MOFs through densification and defect engineering. Unlike traditional approaches relying on pressure or binders,[8] our method focuses on modulating the molecular interactions between MOF nanoparticles. Through chemical interactions, neighboring crystallites are stitched together, leading to enhanced particle adhesion and reduced intergranular voids. By applying this concept to flexible MOFs, we can effectively regulate their flexibility, resulting in remarkable adsorption properties.

It was reported that the densification process in MOFs can trigger various structural changes, such as shearing, deformation, or rearrangement of the crystal lattice, causing alterations in pore structure, shape, and size. A particularly appealing aspect of our densification approach is synchronization, where all MOF particles undergo simultaneous changes. This stands in contrast to pressure-based densification, which may cause uneven structural modifications in the material. This synchronization holds great potential for tailoring gas separation selectivities. For instance, when structural changes occur during pelletization under pressure, they typically affect only the outer layer of the material, leading to differing pore properties between the outer layer and the core of the pellet. Consequently, this uncertainty can result in unclear and uncontrolled selectivity for guest molecules.[9] However, in our densification strategy, the "synchronized" densification-induced structural changes are nearly uniform across all crystals. This uniformity allows us to enhance or even reverse guest selectivity in microporous materials since all crystals react similarly during densification, leading to nearly identical pore properties. Moreover, the tighter particle packing of the densified form not only enhances structural uniformity but also confers an additional advantage by exerting control over gas diffusion into the pores, consequently influencing gas selectivity.

2. Results and Discussion

2.1. The Approach

Defective MOFs represent an emerging subclass with engineered structural defects, such as missing metal ions or organic ligands.[10] These intentional defects can significantly influence the physical and chemical properties of the material, resulting in novel or improved functionalities for various applications like gas storage, separation, catalysis, and sensing. One intriguing aspect of defective MOFs is their structural flexibility. By FS-CuBTC$_{UM}$. incorporating ordered and disordered compartments within the MOF structure, defects induce a degree of lattice flexibility.[11] In this context, we have selected a widely researched, easily synthesized, and commercially available MOF, HKUST-1 or CuBTC MOF, to test our hypothesis. In the realm of gas separation, controlling the structural flexibility of HKUST-1 can significantly influence the separation performance and the interaction with guest molecules.

The MOF was synthesized by mixing copper acetate salt (CuAc) and the 1,3,5-benzene tricarboxylate (BTC) ligand in a mixture of water and ethanol. Additionally, a non-bridging ligand modulator (acetic acid) was introduced during the MOF synthesis. The reaction mixture formed a sky-blue gel instantly at room temperature, and the reaction was then stopped by centrifugation and removal of unreacted starting materials. After washing with ethanol, the material was recentrifuged and resuspended in ethanol. The flat sheets or FS-CuBTC are formed by drop–casting the gel-like material onto a transparent glass sheet and allowing it to dry at room temperature (**Figure 1**).

Each step in the synthesis was carefully optimized for specific purposes. CuAc was chosen as a metal source because it maintains the copper dimer paddlewheel configuration found in HKUST-1, facilitating the quick and straightforward synthesis of the product at room temperature.[12] Acetic acid, like other monotopic acid ligands, acted as a coordination modulator, slowing down the growth of MOF nanoparticles through coordination with and depletion of metal ions. The use of both copper acetate and acetic acid was instrumental in introducing defects into the MOF framework. The fast quenching of the reaction and the specific synthetic conditions were designed to promote the formation of small nanoparticles, which contributes to better packing and enhances the densification process.[13] The coordination of acetic acid with the Cu ions, along with the rapid quenching of the reaction, led to partial coordination of the carboxylate groups of the BTC linkers, leaving free carboxylates of the BTC ligands on the surface of the nanoparticles. These free carboxylatesonthenanoparticlesurfacecouldinteractwithCusitesfrom nearby particles, resulting in particle stitching and improved densification.

Interestingly, despite the success in forming densified MOF materials using our synthetic method, we encountered a challenge in obtaining the MOF in powder form. Filtration was not feasible due to the extremely small particle size of the suspended nanoparticles in ethanol. Regardless of the drying method applied, the nanoparticles always form densified material.

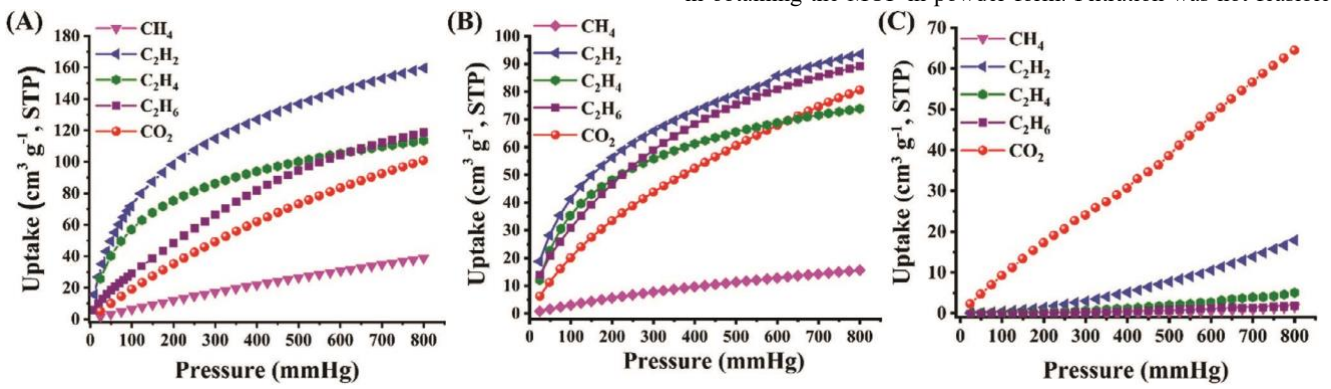

Figure 2. Single-gas adsorption isotherms of CH_4, C_2H_2, C_2H_4, C_2H_6, and CH_4 collected at 298 K for A) CuBTC$_{TWP}$, B) FS-CuBTC (SA = 775), C)

These observations lead us to believe that the interactions between the free carboxylates and metal ions from neighboring particles function as the "mortar" that holds the nanoparticles' "bricks" together. Building on this insight, we hypothesized that removing the mortar-like interactions would allow the "bricks" (particles) to be separated again. In simpler terms, eliminating any unreacted ligand present on the MOF surface might lead to the formation of well-suspended particles, enabling the material to be in powder form.

To test this hypothesis, we carried out several washing steps with extended sonication to thoroughly remove any unreacted species from the surface of the particles. Excitingly, when the thoroughly washed material was dried, it indeed formed a powder that could not be resuspended in ethanol or form densified materials, even after centrifugation. This confirmed our hypothesis that the interactions between the particles play a crucial role in controlling the densification process.

2.2. Characterization

The powder X-ray diffraction (PXRD) analysis of thoroughly washed powder (CuBTC$_{TWP}$) and the as-synthesized flat sheets (FS-CuBTC) exhibited diffraction patterns characteristic of the reported CuBTC material.

Thermal stability assessments of CuBTC$_{TWP}$ and FS-CuBTC were performed using Thermogravimetric Analysis (TGA) in the presence of nitrogen (Figures S1,S2, Supporting Information). The initial weight loss can be attributed to the presence of adsorbed

water molecules in the MOFs. Weight loss at higher temperatures can be linked to the degradation of organic compounds within the MOFs. The breakdown temperature of FSCuBTC (325 °C) was found to be higher than that of $CuBTC_{TWP}$ (300 °C). Thus, FS-CuBTC exhibited higher thermal stability compared to $CuBTC_{TWP}$. This finding was corroborated by PXRD analysis of FS-CuBTC maintained at 320 °C for 1 h, revealing material crystallinity alongside a partial collapse of the structure, as evidenced by a lower intensity peak at 2θ of 6.3 (Figure S3, Supporting Information). The nanoparticles in ethanol ranged

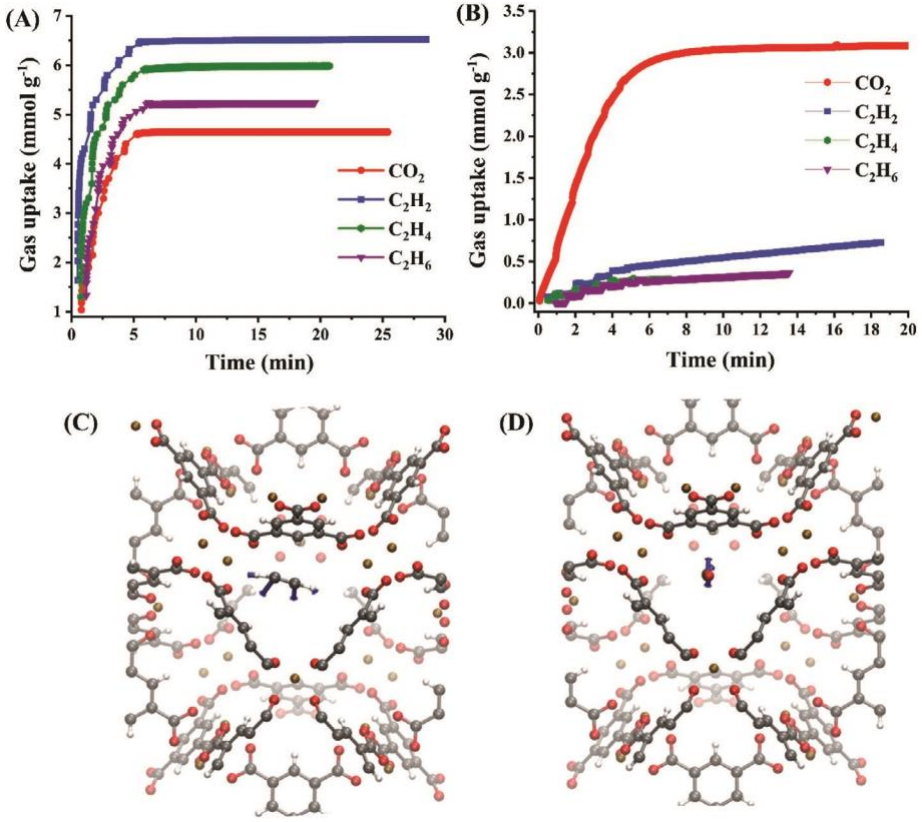

Figure 3. Time-dependent gas uptake profiles of CO_2, C_2H_2, C_2H_4, and C_2H_6 at 1 bar and 298 K in A) $CuBTC_{TWP}$ and B) FS-$CuBTC_{UM}$. C) C_2H_2 and D) CO_2 passing through the smaller tetragonal pore of the FS-$CuBTC_{UM}$, with induced dipoles represented by arrows. C_2H_2 passes horizontally in plane with the pore, and CO_2 passes perpendicular to the pore.

in size from 20 to 60 nm, as determined by transmission electron microscopy (TEM). The TEM study confirmed that the densified material, FS-CuBTC was composed of a single phase of aggregated CuBTC nanoparticles. In contrast, previous TEM imaging of reported CuBTC showed a similar morphology but with significant nano-sized voids (Figure 1C; Figure S4, Supporting Information).

2.3. The Interplay Between Defects, Flexibility, and Densification

To control the flexibility of the densified material, vacuum evacuation was employed as a force to induce a change in the pore properties. TEM images clearly showed that the material exhibited minimal voids between its particles. Given the material's structural flexibility brought on by the presence of weaker walls arising from the presence of defects, any extra stress, such as vacuum evacuation, could perhaps influence the internal pores of the material.

The presence of defects in the densified materials was confirmed through proton nuclear magnetic resonance (^{1}HNMR). The appearance of peaks associated with the three methyl protons in acetate at 1.86 ppm, along with the peaks of the BTC linker in the ^{1}HNMR spectra, clearly indicated the presence of acetate fragments within the structure of FS-CuBTC (Figure S5, Supporting Information). The molar ratio of the acetate fragment to the BTC linker was determined by comparing the three methyl proton peaks of acetate at 1.86 ppm to the three phenyl proton peaks of BTC at 8.55 ppm. The result revealed a BTC:Acetate ratio of approximately 3:1. On the other hand, the ^{1}H NMR profile of the activated $CuBTC_{TWP}$ exhibited a clear signal of BTC ligands, with no detectable signals of the acetate. The $CuBTC_{TWP}$, and FS-CuBTC samples were all activated at 150 °C for 12 h. Subsequently, samples from the same batch of densified material underwent further activation but for an extended period of time under vacuum evacuation at room temperature (see experimental details and Table S1, Supporting Information).

Nitrogen adsorption isotherms were conducted at 77 K, revealing Brunauer–Emmett–Teller (BET) surface areas (SA) of 1406, and 775 $m^2 g^{-1}$ for $CuBTC_{TWP}$, and FS-CuBTC samples activated for 12 h at 150 °C, respectively. Interestingly, after activation at 150°C followed by longer vacuum activation at 25 °C, the FSCuBTC showed no N_2 uptake at 77 K while the $CuBTC_{TWP}$ exhibited a BET

surface area of 1273 m^2 g^{-1}. Nevertheless, the CO_2 adsorptionisothermscollectedat298Kdemonstratednearlysimilar uptakes for both the samples activated for a shorter time and those activated for a longer time, revealing that the materials remain porous despite their N_2 uptake at 77 K (Figures S7,S8, Supporting Information).

For a more in-depth analysis of structural crystallinity,

	CuBTC$_{TWP}$			FS-CuBTC$_{UM}$		
Gas Selectivity	Uptake Ratio @1 bar	IAST (50:50)	IAST (1:99)	Uptake Ratio @1 bar	IAST (50:50)	IAST (1:99)
CO_2/C_2H_2	0.62	0.2	0.23	4	4	7
CO_2/C_2H_4	0.87	0.28	0.33	15.5	15	21
CO_2/C_2H_6	0.84	0.61	0.62	41	4416	45
CO_2/CH_4	2.6	3.5	3.4	50	135	56

powderX-ray diffraction (PXRD) was conducted. Pawley refinement confirmedthepresenceofpeaksplittingsandshiftsintheFS-CuBTC sample activated for a longer time in comparison to the assynthesized analogs and the simulated pattern (Figure 1E; Figure S6, Supporting Information). The data revealed that the lattice symmetry is reduced from cubic to tetragonal, which validates that the framework undergoes a drastic shearing process to minimize the void space within the structure (Table S2, Supporting Information). The shearing process leads to a downsizing of the pores, resulting in the formation of an ultramicroporous (UM) CuBTC variant, namely FS-CuBTC$_{UM}$. Initially, we thought there might be a temperature-triggered structural change, but comparing the PXRD patterns at various temperatures revealed no significant alterations in the structure. Instead, as the pore size decreases, kinetic barriers are generated, which are particularly prominent at low temperatures. These barriers make it challenging for certain gases, such as N_2, to pass through small pores.

As a result, the gas adsorption behavior of the MOFs observed at cryogenic temperatures may not follow the same trends at room temperature. The FS-CuBTC$_{UM}$ exhibits no CO_2 uptake at 195 K, indicating the presence of kinetic barriers within this temperature range. In light of this, the term "kinetically closed pore" may aptly describe the newly formed pores in FS-CuBTC$_{UM}$. This implies that gas diffusion into these ultramicropores is impeded unless the gas possesses sufficient kinetic energy to overcome the diffusion barrier, as previously observed in other MOFs with ultramicropores.[14]

2.4. CO_2/C2 Hydrocarbons Separation

As mentioned earlier, typical physisorbed materials exhibit a preference for unsaturated hydrocarbons over CO_2. Consistently, CuBTC$_{TWP}$ and FS-CuBTC activated at 150 °C for 12 h, demonstrated selective adsorption of C_2H_2, C_2H_4, and C_2H_6 over CO_2. In these frameworks, the presence of sufficiently large pores enables almost equal and unrestricted diffusion of gases, with gas selectivity primarily dependent on the interaction of the gas with the framework.

Interestingly, when a vacuum is applied for a longer time on the same samples, the hydrocarbon/CO_2 selectivity is reversed, leading to CO_2-selective FS-CuBTC$_{UM}$ over C_2 hydrocarbons (**Figure 2**). The observed low affinity and inverted selectivity of FS-CuBTC$_{UM}$ toward more polarizable hydrocarbons are noteworthy. This material demonstrates excellent performance with almost no adsorption for C_2H_6, C_2H_4 and CH_4. The uptake ratios (UR) at 1 bar for CO_2/C_2H_6, CO_2/C_2H_4, CO_2/C_2H_2, and CO_2/CH_4 are 41, 15.5, 4, and 50, respectively, which outperform many materials previously recognized for their CO_2 preference over hydrocarbons (**Table 1**; Figures S3,S4, Supporting Information).[4] Ideal Adsorbed Solution Theory (IAST) calculations revealed that FS-CuBTC$_{UM}$ exhibits superb CO_2 over hydrocarbon selectivities at 1 bar and 298 K as shown in Table 1, TablesS3,S4,FiguresS9–S16(SupportingInformation).Interestingly, a striking improvement in CO_2 over C_2H_6 selectivity was observed in FS-CuBTC$_{UM}$ (S_{UR} = 41 and $S_{IAST(50:50)}$ = 4416) at 298 K and 1 bar, surpassing the performance of benchmark materials, MUF-16 (15.6 and 600),[15] and [Zn(odip)$_{0.5}$(bpe)$_{0.5}$] (4.3 and 27.9).[16] FS-CuBTC$_{UM}$ is thus the best physisorbent known for this separation. Indeed, it is common for many MOFs to

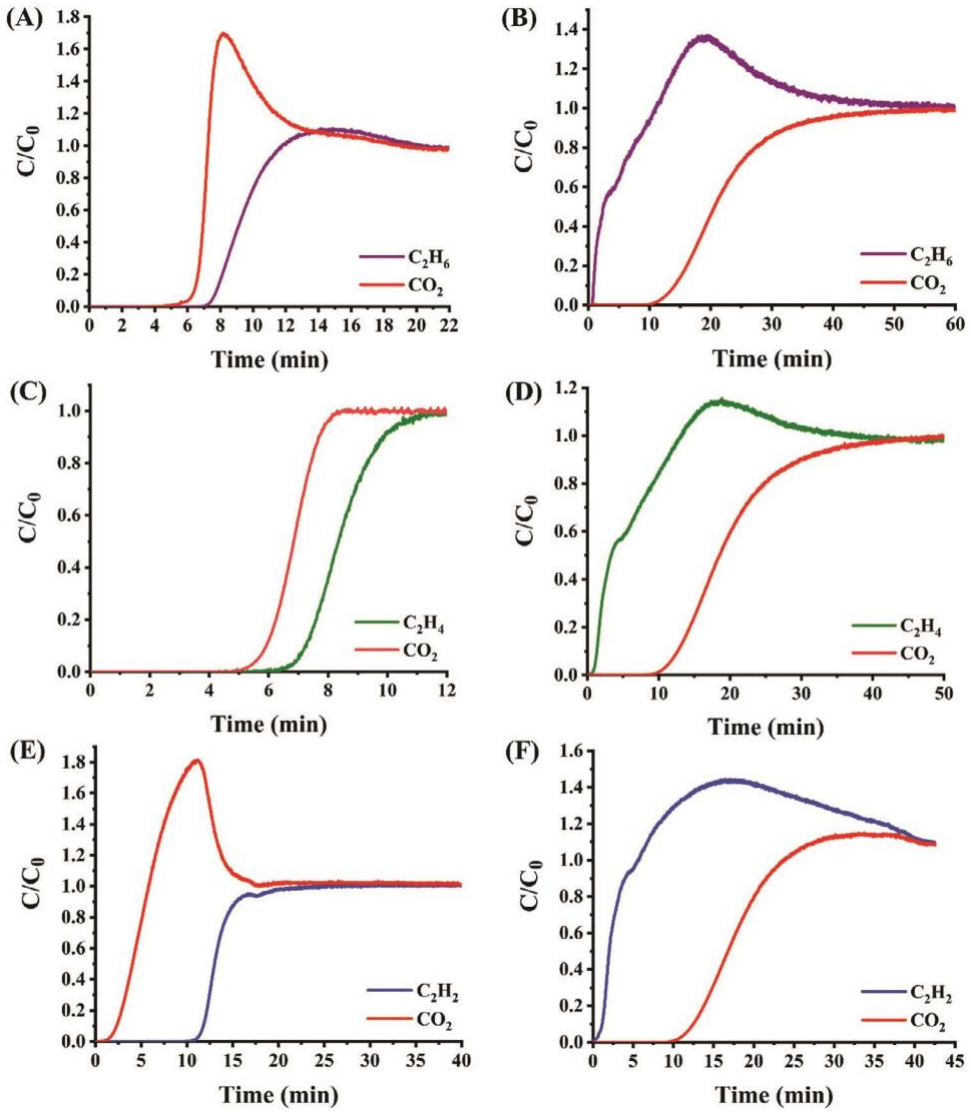

Figure 4. Column breakthrough curves of 1:1 binary mixture of A) CO_2/C_2H_6 for $CuBTC_{TWP}$, B) CO_2/C_2H_6 for FS-$CuBTC_{UM}$, C) CO_2/C_2H_4 for $CuBTC_{TWP}$, D) CO_2/C_2H_4 for FS-$CuBTC_{UM}$, E) CO_2/C_2H_2 for $CuBTC_{TWP}$, and F) CO_2/C_2H_2 for FS-$CuBTC_{UM}$.

exhibit similar adsorption capacities for CO_2, C_2H_2, and C_2H_4, resulting in low CO_2/C_2H_2 and CO_2/C_2H_4 selectivity, a characteristic shared by $CuBTC_{TWP}$ and FS-CuBTC activated for a shorter time. However, these selectivities are reversed with an outstanding improvement in CO_2 over C_2H_4 selectivity (S_{UR} = 15.5) observed in FS-$CuBTC_{UM}$ at 298 K and 1 bar, exceeding benchmarks like 5A Zeolite (1.2),[17] Mg–MOF-74 (1.1),[18] $[Zn(odip)_{0.5}(bpe)_{0.5}]$ (1.4),[16] ZJU-197 (2.2),[19] SU-101(Al) (2.5),[20] QC-5-Cu (3.3)[21] and MUF-16 (15)[15] and is surpassed by only one other reported adsorbent (F-PYMO-Cu).[22] Although $CuBTC_{TWP}$ showed CO_2/CH_4 selectivity (S_{UR} = 2.6), however, this selectivity is further improved in FS-$CuBTC_{UM}$ (50), which is considered one of the best materials for CO_2/CH_4 separation, only surpassed by SIFSIX-14-Cu-i (85).[23] This enhanced performance can be attributed to the small pores and reduced interparticle gaps postdensification, promoting a higher affinity for CO_2 over hydrocarbons.

As the pore size decreases, gas diffusion is significantly impeded due to the confined space, rendering the material more selective toward gases that can enter the pores more freely, such as CO_2.[24] The gas diffusion here is not solely governed by the confined space but is also influenced by the minimal spaces between particles, a result of their interaction facilitating better adhesion. This densification protocol, while promoting better packing, can impede the diffusion of gas, hindering its travel from the monolithic surface to the depth of the material. This prompts a more in-depth exploration of the kinetic adsorption properties of FS-$CuBTC_{UM}$ in comparison to $CuBTC_{TWP}$. Analyzing the timedependent uptake profiles (**Figure 3**) allows for a deeper investigation into the diffusion of gases from the bulk to the pores of the materials.

The diffusional time constant, D', calculated for all gases (as detailed in the supporting information), indicates a noteworthy finding. The kinetic studies reveal that FS-CuBTC$_{UM}$ exhibits

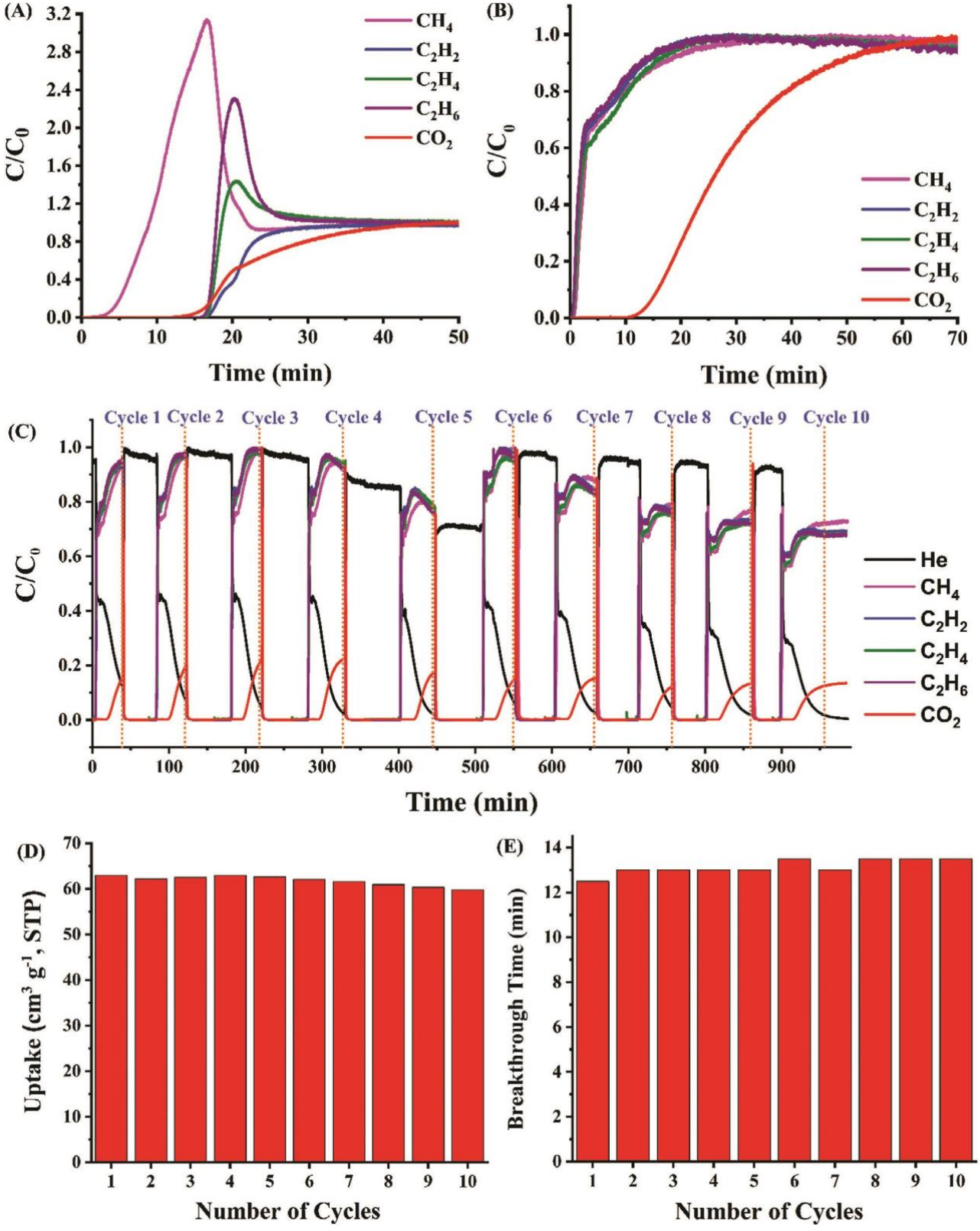

Figure 5. Column breakthrough curves and recycling experiments of equimolar quinary mixture of CH_4, C_2H_2, C_2H_4, C_2H_6, and CO_2 for A) $CuBTC_{TWP}$, and B) FS-$CuBTC_{UM}$ at 298 K and total pressure of 1 bar, C) 10 cycles of breakthrough experiments (10 adsorption and room temperature purging stages). D) cycle adsorption tests of CO_2 captured in FS-$CuBTC_{UM}$ at 298 K were collected using an adsorption gas analyzer. E) cycle dynamic tests collected using breakthrough experiments with a packed bed of FS-$CuBTC_{UM}$.

a significantly faster diffusion rate for CO_2 compared to all hydrocarbons, establishing FS-$CuBTC_{UM}$ as a CO_2-preferential adsorbent in terms of kinetic factors and demonstrating resistance to hydrocarbon diffusion. In contrast, $CuBTC_{TWP}$ exhibits a comparable diffusional time constant for all gases, signifying poor kinetic selectivity (Figure 3A,B; Figures S17,S18, Table S5, Supporting Information).

Reducing the pore size, as seen in the densified FS-$CuBTC_{UM}$, has a crucial impact on CO_2/C_2H_4 and C_2H_6 selectivity, potentially reversing it due to the larger size and molecular shape of C_2H_4 andC_2H_6,slowingtheirdiffusionintothepore.Incontrast, CO_2 and C_2H_2, with similar properties, have historically posed challenges in separation. To gain further insights into the slower diffusion of C_2H_2 compared to CO_2, simulation studies were conducted to assess their adsorption by FS-$CuBTC_{UM}$. Simulations were performed in the NVT ensemble at a temperature of 298 K and timestep of 2 fs with OpenMM 8.0. Both sorbates and MOF were parameterized with the PHAST2 forcefield, which includes explicitly induced dipole polarization. Experimental crystal structures were employed and the MOF was assumed to be rigid. During the simulation, C_2H_2 passed through horizontally in a plane with the pore, while CO_2 passed through perpendicular to the pore. Both sorbates show induced dipole interactions with nearby carbons, oxygens, and hydrogens from the BTC linkers that forced these orientations. Despite their similar properties, CO_2 and C_2H_2 have inverted quadrupole moments that allow CO_2 to pass from bulk into the material faster at the surface than acetylene (as shown in Figure 3C,D), though once in the material C_2H_2 has a higher diffusivity. Conclusively, the integration of experimental and theoretical investigations underscores the capability of the densified MOF to effectively separate CO_2 from hydrocarbons through a synergistic interplay of size-exclusion and kinetic separation mechanisms.

Given the improved selectivity of FS-$CuBTC_{UM}$ for CO_2 over hydrocarbons, we conducted breakthrough experiments to evaluate its dynamic separation performance for a CO_2/hydrocarbon binary gas mixtures (1/1, v/v) at 298 K. To ensure a fair comparison, we tested both FS-$CuBTC_{UM}$ and $CuBTC_{TWP}$ samples from the same batch, and the data was also replicated using different batches for validation.

The results depicted in **Figure 4**A,C,E confirmed that $CuBTC_{TWP}$ selectively adsorbs hydrocarbons over CO_2, consistent with previous observations for CuBTC powder. CO_2 was the first to elute from $CuBTC_{TWP}$, while C_2H_2, C_2H_4, and C_2H_6 broke through the column later. In contrast, FS-$CuBTC_{UM}$ exhibited a different behavior, with CO_2 breakthrough occurring at approximately 10 min, while the hydrocarbons (C_2H_2, C_2H_4, and C_2H_6) rapidly passed through the adsorption bed at the beginning of the experiment (Figure 4B,D,F). This outcome further supports the great potential of FS-$CuBTC_{UM}$ for practical dynamic gas separation.

Remarkably, FS-$CuBTC_{UM}$ demonstrated exceptional CO_2 separation performance even in an equimolar quinary gas mixture of CO_2, C_2H_2, C_2H_4, C_2H_6, and CH_4 (**Figure 5**). In this scenario, only negligible amounts of hydrocarbons were adsorbed in FSCuBTC$_{UM}$, and they quickly eluted, while the CO_2 remained in the column. Conversely, $CuBTC_{TWP}$ was unable to separate CO_2 from C2 hydrocarbons in the quinary gas mixture. The difference in breakthrough time between CO_2 and C2 hydrocarbons was only 1–2 min, likely due to competitive adsorption of gases in the MOF pores. Cyclic experiments, involving the collection of gas adsorption isotherms and breakthrough experiments, were employed to assess the reusable life of FS-$CuBTC_{UM}$. The regeneration process involved pulling a vacuum for a few minutes or flushing helium for 30–45 min at room temperature. Remarkably, even after ten cycle tests, there was no significant decrease observed in CO_2 uptake and breakthrough time (as depicted in Figure 5C–E), affirming the material's commendable regeneration ability and stability. The preferential adsorption of CO_2 over C1 and C2 hydrocarbons (both saturated and unsaturated) by FSCuBTC$_{UM}$ allows for the direct production of high-purity light hydrocarbon feedstocks, highlighting its promising potential in practical gas separation applications.

3. Conclusion

In conclusion, this study introduces an innovative strategy for controlling the flexibility of MOFs through densification and defect engineering. The approach involves deliberated introduction of structural defects within the MOF lattice, inducing a degree of lattice flexibility. By modulating the interactions between the nanoparticles of the defective CuBTC MOF, the particle adhesion is improved and the intergranular voids are reduced. Further densification achieved during vacuum activation triggers the shearing of the crystals from cubic to tetragonal, and the contraction of the pores across nearly all crystals. Experimental kinetic studies and simulations demonstrate that the confined space and minimal interparticle gaps in FS-$CuBTC_{UM}$ result in superior gas selectivity, particularly with accelerated CO_2 diffusion over hydrocarbons through kinetic and size-exclusion mechanisms. This unique behavior leads to remarkable CO_2/C_2H_6, CO_2/C_2H_4, and CO_2/CH_4 selectivity, surpassing other state-ofthe-art MOFs. The application of this strategy in gas separation is highly promising, as demonstrated by the exceptional performance of the densified CuBTC flat sheets in dynamic gas separation experiments. Even in quinary gas mixtures, the densified material efficiently separates CO_2 from hydrocarbons, overcoming the challenges posed by competitive adsorption in MOFs including reported CuBTC. This novel approach also offers a significant advantage over conventional methods, as it eliminates the need for two energy-intensive steps of adsorption and desorption, making it an energy-efficient alternative for gas separation processes.

Supporting Information

Supporting Information is available from the Wiley Online Library or from the author.

Acknowledgements

S.E. and W.X. gratefully acknowledge funding support from the U.S. DOEOffice of Basic Energy Sciences under Contract No. DE-SC0024594. Part of this research used resources of the Advanced Photon Source, a U.S. Department of Energy (DOE) Office of Science user facility at Argonne National Laboratory, and is based on research supported by the U.S. DOE Office of Science-Basic Energy Sciences, under Contract No. DE-AC0206CH11357. This work also made use of the IMSERC Crystallography facility at Northwestern University, which has received support from the Soft and Hybrid Nanotechnology Experimental (SHyNE) Resource (NSF ECCS-2025633), and Northwestern University. This material is also based upon work supported by the National Science Foundation under Grant No. 2154882 and the National Science Foundation Graduate Research Fellowship Program under Grant No. DGE-2137100. B.S. also acknowledges computing time from High-Performance Computing at NC State and ACCESS under Grant No. CHE230105.

Conflict of Interest

The authors declare no conflict of interest.

Author Contributions

S.E. and M.M performed the conceptualization. M.M., I.E., J.S., Y.P, W.X., C.M. T. P., L.M., and A.H., developed the methodology. M.M. and S.E. performed the investigation. S.E., M.M., D.H., and B.S. performed the supervision. M.M. wrote the original draft. S.E., I.E., J.S., W.X., and Y.P. wrote, reviewed, and edited the final draft.

Data Availability Statement

The data that support the findings of this study are available from the corresponding author upon reasonable request.

Keywords

CO_2-hydrocarbon separation, CuBTC, defect engineering, densification, metal–organic frameworks, monoliths

Received: October 6, 2023
Revised: December 31, 2023
Published online:

[1] D. S. Sholl, R. P. Lively, *Nature* **2016**, *532*, 435.
[2] M. Takht Ravanchi, S. Sahebdelfar, *Appl. Petrochem. Res.* **2014**, *4*, 63.
[3] a) C.-H. Yu, C.-H. Huang, C.-S. Tan, *Aeros. Air Qual. Res.* **2012**, *12*, 745; b) D. M. D'alessandro, B. Smit, J. R. Long, *Angew. Chem., Int. Ed.* **2010**, *49*, 6058; c) S.-Y. Lee, S.-J. Park, *J. Ind. Eng. Chem.* **2015**, *23*, 1.
[4] H. Huang, L. Wang, X. Zhang, H. Zhao, Y. Gu, *Clean Technol.* **2022**, *5*, 1.
[5] M. L. Foo, R. Matsuda, Y. Hijikata, R. Krishna, H. Sato, S. Horike, A. Hori, J. Duan, Y. Sato, Y. Kubota, M. Takata, S. Kitagawa, *J. Am. Chem. Soc.* **2016**, *138*, 3022.
[6] L.-N. Ma, G.-D. Wang, L. Hou, Z. Zhu, Y.-Y. Wang, *ACS Appl. Mater. Interfaces* **2022**, *14*, 26858.
[7] J. Duan, M. Higuchi, M. L. Foo, S. Horike, K. P. Rao, S. Kitagawa, *Inorg. Chem.* **2013**, *52*, 8244.
[8] a) U. H. Lee, S. K. Chitale, Y. K. Hwang, J.-S. Chang, in *Metal-Organic Frameworks in Biomedical and Environmental Field*, (Eds: P. H Cortés, S. Rojas Macías), Springer International Publishing, Cham **2021**; b) J. Hou, A. F. Sapnik, T. D. Bennett, *Chem. Sci.* **2020**, *11*, 310; c) X. Qi, K. Liu, Z. Chang, *Chem. Eng. J.* **2022**, *441*, 135953; d) B. M. Connolly, D. G. Madden, A. E. H. Wheatley, D. Fairen-Jimenez, *J. Am. Chem. Soc.* **2020**, *142*, 8541.
[9] a) C. L. Hobday, R. J. Marshall, C. F. Murphie, J. Sotelo, T. Richards, D. R. Allan, T. Düren, F.-X. Coudert, R. S. Forgan, C. A. Morrison, S. A. Moggach, T. D. Bennett, *Angew. Chem., Int. Ed.* **2016**, *55*, 2401; b) S. Yuan, X. Sun, J. Pang, C. Lollar, J.-S. Qin, Z. Perry, E. Joseph, X. Wang, Y. Fang, M. Bosch, D. Sun, D. Liu, H.-C. Zhou, *Joule* **2017**, *1*, 806; c) G. K. H. Shimizu, *Chem* **2017**, *3*, 924; d) T. D. Bennett, P. Simoncic, S. A. Moggach, F. Gozzo, P. Macchi, D. A. Keen, J.-C. Tan, A. K. Cheetham, *Chem. Commun.* **2011**, *47*, 7983; e) R. N. Widmer, G. I. Lampronti, S. Chibani, C. W. Wilson, S. Anzellini, S. Farsang, A. K. Kleppe, N. P. M. Casati, S. G. Macleod, S. A. T. Redfern, F.-X. Coudert, T. D. Bennett, *J. Am. Chem. Soc.* **2019**, *141*, 9330; f) P. Vervoorts, J. Stebani, A. S. J. Méndez, G. Kieslich, *ACS Mater. Lett.* **2021**, *3*, 1635; g) I. E. Collings, A. L. Goodwin, *J. Appl. Phys.* **2019**, *126*, 181101.
[10] a) A. F. Möslein, L. Donà, B. Civalleri, J.-C. Tan, *ACS Appl. Nano Mater.* **2022**, *5*, 6398; b) S. Dissegna, K. Epp, W. R. Heinz, G. Kieslich, R. A. Fischer, *Adv. Mater.* **2018**, *30*, 1704501; c) J. Ren, M. Ledwaba, N. M. Musyoka, H. W. Langmi, M. Mathe, S. Liao, W. Pang, *Coord. Chem. Rev.* **2017**, *349*, 169.
[11] T. D. Bennett, A. K. Cheetham, A. H. Fuchs, F.-X. Coudert, *Nat. Chem.* **2017**, *9*, 11.
[12] U. Ryu, S. Jee, P. C. Rao, J. Shin, C. Ko, M. Yoon, K. S. Park, K. M. Choi, *Coord. Chem. Rev.* **2021**, *426*, 213544.
[13] a) Y. Sakata, S. Furukawa, M. Kondo, K. Hirai, N. Horike, Y. Takashima, H. Uehara, N. Louvain, M. Meilikhov, T. Tsuruoka, S. Isoda, W. Kosaka, O. Sakata, S. Kitagawa, *Science* **2013**, *339*, 193; b) A. Umemura, S. Diring, S. Furukawa, H. Uehara, T. Tsuruoka, S. Kitagawa, *J. Am. Chem. Soc.* **2011**, *133*, 15506; c) S. Wannapaiboon, K. Sumida, K. Dilchert, M. Tu, S. Kitagawa, S. Furukawa, R. A. Fischer, *J. Mater. Chem. A* **2017**, *5*, 13665; d) A. L. Semrau, Z. Zhou, S. Mukherjee, M. Tu, W. Li, R. A. Fischer, *Langmuir* **2021**, *37*, 6847; e) S. K. Elsaidi, M. Ostwal, L. Zhu, A. Sekizkardes, M. H. Mohamed, M. Gipple, J. R. Mccutcheon, D. Hopkinson, *RSC Adv.* **2021**, *11*, 25658; f) S. K. Elsaidi, S. Venna, A. K. Sekizkardes, J. A. Steckel, M. H. Mohamed, J. Baker, J. Baltrus, D. Hopkinson, *Cell Rep. Phys. Sci.* **2020**, *1*, 100113; g) S. K. Elsaidi, S. R. Venna, M. H. Mohamed, M. J. Gipple, D. P. Hopkinson, *Cell Rep. Phys. Sci.* **2020**, *1*, 100059.
[14] a) H. Kim, D. G. Samsonenko, M. Yoon, J. W. Yoon, Y. K. Hwang, J.-S. Chang, K. Kim, *Chem. Commun.* **2008**, 4697; b) T. X. Nguyen, S. K. Bhatia, *J. Phys. Chem. C* **2007**, *111*, 2212.
[15] O. T. Qazvini, R. Babarao, S. G. Telfer, *Nat. Commun.* **2021**, *12*, 197.
[16] S. Horike, K. Kishida, Y. Watanabe, Y. Inubushi, D. Umeyama, M. Sugimoto, T. Fukushima, M. Inukai, S. Kitagawa, *J. Am. Chem. Soc.* **2012**, *134*, 9852.

[17] I. Van Zandvoort, J. K. Van Der Waal, E.-J. Ras, R. De Graaf, R. Krishna, *Sep. Purif. Technol.* **2019**, *227*, 115730.
[18] a) Z. Bao, S. Alnemrat, L. Yu, I. Vasiliev, Q. Ren, X. Lu, S. Deng, *Langmuir* **2011**, *27*, 13554; b) J. Yu, P. B. Balbuena, *J. Phys. Chem. C* **2013**, *117*, 3383.
[19] L. Zhang, K. Jiang, Y. Yang, Y. Cui, B. Chen, G. Qian, *J. Solid State Chem.* **2017**, *255*, 102.
[20] C. Hao, H. Ren, H. Zhu, Y. Chi, W. Zhao, X. Liu, W. Guo, *Sep. Purif. Technol.* **2022**, *290*, 120804.
[21] T. He, Y. Xiao, Q. Zhao, M. Zhou, G. He, *Ind. Eng. Chem. Res*. **2020**, *59*, 3153.
[22] X. Jiang, T. Pham, J.-W. Cao, K. A. Forrest, H. Wang, J. Chen, Q.-Y. Zhang, K.-J. Chen, *Chem. Eur. J.* **2021**, *27*, 9446.
[23] M. Jiang, B. Li, X. Cui, Q. Yang, Z. Bao, Y. Yang, H. Wu, W. Zhou, B. Chen, H. Xing, *ACS Appl. Mater. Interfaces* **2018**, *10*, 16628.
[24] a) C. He, P. Zhang, Y. Wang, Y. Zhang, T. Hu, L. Li, J. Li, *Sep. Purif. Technol.* **2023**, *304*, 122318; b) Y. Wang, D. Zhao, *Cryst. Growth Des.* **2017**, *17*, 2291; c) J. Cui, Z. Qiu, L. Yang, Z. Zhang, X. Cui, H. Xing, *Angew. Chem.* **2022**, *134*, e202208756.